

Locating the avalanche structure and the origin of breakdown generating charge carriers in silicon photomultipliers by using the bias dependent breakdown probability

Adam Nepomuk Otte^{a,*}, Thanh Nguyen^a, Joel Stansbury^a

^a*School of Physics & Center for Relativistic Astrophysics, Georgia Institute of Technology,
837 State Street NW, Atlanta, GA 30332-0430, USA.*

Abstract

We present characterization results of two silicon photomultipliers; the Hamamatsu LVR-6050-CN and the Ketek PM3325 WB. With our measurements of the bias dependence of the breakdown probability we are able to draw conclusions about the location and spatial extension of the avalanche region. For the KETEK SiPM we find that the avalanche region is located close to the surface. In the Hamamatsu SiPM the high-field region is located $0.5\ \mu\text{m}$ below the surface, while the volume above is depleted almost until the surface. Furthermore, for the Hamamatsu SiPM we find that charge carriers produced by optical-crosstalk photons enter a cell below the avalanche region as opposed to an earlier device where most of the photons enter a cell from above. In the here tested Hamamatsu device the crosstalk photons probably absorb in the bulk and the generated holes diffuse into the active volume of the cell within 2 ns and initiate a breakdown. The present paper is an attempt to spur further interest in the use of the bias dependence of the breakdown probability and establish it as a standard tool not only to determine the location of the high-field region but also to determine the origin of charge carriers relative to the high-field region. With the knowledge of where the charges come from it should be possible to further improve the optical crosstalk, dark count, and afterpulsing characteristics of SiPM.

Keywords: Semiconductor devices, Silicon Photomultipliers, SiPMs, Geiger-mode APDs, Semiconductor detectors, Semiconductor device modeling, Silicon devices, Photodetectors

1. Introduction

The silicon photomultiplier (SiPM) has evolved into an established photodetector technology. They are used in high-energy physics [1, 2, 3], astroparticle physics [4, 5], medical imaging [6, 7], and LIDARs [8, 9], to only name a few areas of application. One key factor to the success of SiPMs is the continuing effort made by manufacturers to reduce nuisance parameters like dark-count rate, afterpulsing, and optical crosstalk.

Diagnostic tools are crucial in these efforts as they help to identify means that further reduce nuisance parameters, which in turn, improves the performance of SiPMs. One way to diagnose SiPMs is to measure their characteristics as function of temperature and bias, model the data, and extract physical meaningful quantities from the model parameters. We have taken that approach in earlier work [10] and we use it again here.

In this paper we emphasize the use of the bias dependence of the breakdown probability, which we already used in [10] to determine the origin of optical crosstalk in a Hamamatsu device and extend it to a discussion of the location of the avalanche region. While the approach is not

new, e.g. it is used in [11] to characterize FBK devices, we propose to use a different parameter, which is inherently less dependent on the device specifics and thus allows a direct comparison of different devices.

2. Devices used in this Study

The Hamamatsu SiPM is a prototype named LVR2-6050-CN. The device has an active area of $6 \times 6\ \text{mm}^2$ and is composed of $50\ \mu\text{m}$ sized cells. For better UV sensitivity the sensor is not covered with a protective layer. The bias voltage at room temperature to achieve a breakdown probability of 90% when illuminated with 400 nm photons is about 42 V (see later). This is less than the 56 V required for the Hamamatsu LCT5 device we tested in [10]. The breakdown voltage is 38.4 V. The lower bias can possibly be attributed to an about 30% narrower high-field region in the present device if an avalanche region with constant electric field and otherwise similar technology is assumed ($1 - 56\ \text{V}/42\ \text{V} \sim 0.3$).

The second device is a KETEK PM3325 WB SiPM. It has an active area of $3 \times 3\ \text{mm}^2$ and $25\ \mu\text{m}$ cells. The chip is protected with a $400\ \mu\text{m}$ thick glass window. The PM3325 does not feature trenches to suppress optical crosstalk. The bias voltage to achieve a 90% breakdown probabil-

*Corresponding author

Email address: otte@gatech.edu (Adam Nepomuk Otte)

ity when illuminated with 400 nm photons is about 32 V, with a breakdown voltage of 27.5 V at room temperature.

3. Probing the Avalanche Structure with Photon Detection Efficiency Measurements

The photon detection efficiency (PDE) is one example where the breakdown probability plays a decisive role. Depending on the photon's absorption length and the location and extension of the high-field region, a photon is either absorbed above the high-field region (blue photons) or below it (red photons). The photon absorption results in the generation of an electron and hole, which—in case the absorption takes place in the active volume of the cell—drift in opposite directions due to the electric field in the depleted volume. If the photon absorbs below the high-field region in a *p*-on-*n* structure, it is the hole that drifts into the high-field region, if the photon absorbs above the high-field region, it is the electron that drifts down into the avalanche region.

The probability to initiate a Geiger breakdown is smaller for holes than for electrons (due to the lower mobility of holes in silicon, e.g. [12]). One would, therefore, reverse engineer the location and vertical extension of the high-field region if one could measure the probability of a subsequent breakdown as a function of where the electron/hole pair is released.

Such a mapping is indeed possible with bias dependent PDE measurements as has been shown in [11]. For the Hamamatsu SiPM we measured the PDE at three wavelengths and for the KETEK device at four wavelengths. A description of the setups and procedures used for the PDE and all other measurements presented here is given in [10].

Like in our previous measurements we find that the PDE for a given wavelength is well fit with the empirical model

$$PDE(U_{\text{rel}}) = PDE_{\text{max}} [1 - e^{-\mathcal{O} \cdot U_{\text{rel}}}], \quad (1)$$

where $U_{\text{rel}} = (U - U_{\text{BD}}) / U_{\text{BD}}$ is the relative overvoltage above the breakdown voltage U_{BD} . PDE_{max} is called the PDE in saturation but is not necessarily the true saturation value because we cannot measure the PDE at higher bias values. The term in square brackets is the breakdown probability, which depends only on the product of the relative overvoltage and a dimensionless parameter \mathcal{O} , which is mostly dependent on whether an electron or a hole initiates a breakdown as we explain later.¹

In that context it is interesting to remark that empirically all the bias dependent physics of the breakdown is included in one single constant, or in a linear function when larger relative overvoltages than measured here are taken into account [11]. Because our data is well described with

one constant we do not need to consider the linear function, which would, furthermore, not be sufficiently constrained by our data. The devices we tested cannot be operated much beyond the measured voltage range.

While the overall fit function is the same as in [11] there are two differences in its usage that are worth pointing out. Firstly, we use the relative instead of the absolute voltage. Secondly, we choose to map the physical meaningful \mathcal{O} as the parameter instead of the absolute bias voltage at which the PDE reaches 95%. Both choices bring certain advantages.

The relative overvoltage is proportional to \bar{E} , the average electrical field above breakdown in the avalanche region and is normalized to \bar{E}_{BD} , the average electrical field at breakdown.

$$U_{\text{rel}} = \frac{U - U_{\text{BD}}}{U_{\text{BD}}} = \frac{\bar{E} \cdot w - \bar{E}_{\text{BD}} \cdot w}{\bar{E}_{\text{BD}} \cdot w} = \frac{\bar{E} - \bar{E}_{\text{BD}}}{\bar{E}_{\text{BD}}} \quad (2)$$

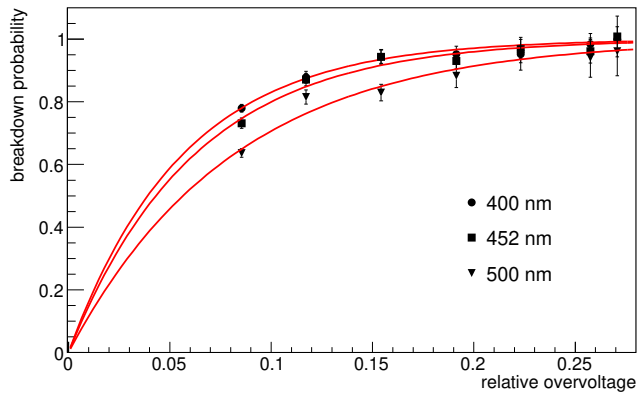
Thus, the relative overvoltage does not depend on the width of the avalanche region w , which drops out in the above equation for devices where the width of the depleted region does not change between breakdown and operating voltage. That assumption holds true for most available SiPM including the tested devices where no or little bias dependence of the cell capacitance is measured².

The avalanche and breakdown characteristics of a pn-junction are governed by the ionization rates, which depend strongest on the electrical field and much less on device specifics like the doping profile and doping concentrations or temperature [13]. The electrical field and thus U_{rel} is, therefore, a natural physical quantity to use in the parameterization of any breakdown dependent quantity. Furthermore, the normalization to \bar{E}_{BD} compensates for some, but admittedly, not all of the device specific dependencies. When comparing different devices, U_{rel} is thus a much better choice than the absolute overvoltage and any differences between devices provides insight into differences in the structures. A good example, where using U_{rel} makes a difference, is the study of the temperature dependence of an SiPM feature measured at different temperatures on the same device. By plotting such a quantity vs. U_{rel} , the temperature dependence of the breakdown voltage is compensated for and any residual temperature dependence can be attributed to physical mechanisms, which are not related to the avalanche process. Our optical crosstalk and afterpulsing measurements we discuss later are such examples.

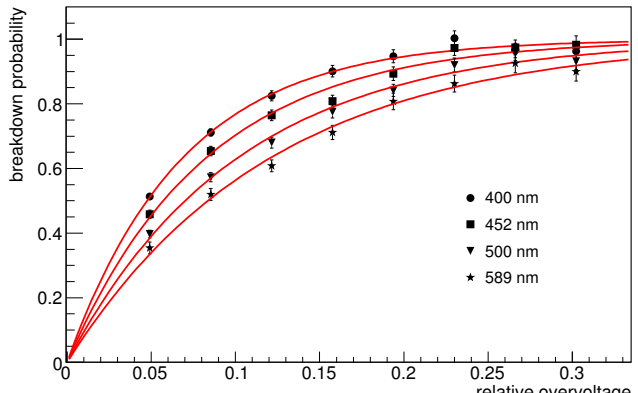
Figure 1 shows the breakdown probability derived from the PDE measurements, i.e. the PDE divided by PDE_{max} . The solid lines depict the best fit parameterizations of the breakdown probability, which all yield fit probabilities of 30% or better. The fitted values of \mathcal{O} are listed in Table 1 together with the corresponding photon absorption lengths. The 589 nm light source was not available for the measurement of the Hamamatsu device.

¹ \mathcal{O} was jocularly referred to as the *Otte number* at recent meetings.

²That is the slope in gain vs. bias measurements.



(a) Hamamatsu LVR2



(b) KETEK PM3325

Figure 1: Breakdown probability versus relative overvoltage for the two tested devices. The lines are fits to the data points with the model described in the text.

Table 1: Values of \mathcal{O} derived from PDE measurements at different wavelength for the two devices. The second column gives the absorption length of photons with the wavelength given in the first column.

Wavelength [nm]	Absorp. length [μm]	\mathcal{O}	
		Hamamatsu	KETEK
400	0.082	17.7 ± 0.6	14.6 ± 0.3
452	0.43	16.1 ± 0.6	12.1 ± 0.3
500	0.91	12.3 ± 0.4	9.9 ± 0.2
589	2.0	N/A	8.3 ± 0.2

The value of \mathcal{O} decreases with increasing photon wavelength for each device, which is a testimony to the fact that the breakdown probability shifts from majority electron to majority hole initiated breakdowns. Bluer photons absorb mostly *above* the avalanche region and it is the electron of the electron/hole pair that drifts into the avalanche region in *p*-on-*n* devices like the ones studied here. Longer wavelength photons are more likely to absorb *below* the avalanche region in which case it is the hole that drifts back up into the avalanche region. \mathcal{O} thus depends on the ratio of electron to hole initiated breakdowns. It should also depend on the spatial extent of the avalanche region in depth and width but we could not explore this aspect further because we lack sufficient knowledge of the avalanche structure.

For the time being, we resort to the assumption that the dependence of \mathcal{O} on the width of the avalanche region is small compared to the observed change with photon-wavelength and can be neglected. How valid that assumption actually is needs to be shown in a future study. In fact, the avalanche regions of the two devices have fairly similar widths, which we infer from the similarities of their respective breakdown voltages, which are 26.8 V and 37.5 V at 0 °C for the KETEK and Hamamatsu SiPM, respectively.

For the Hamamatsu device \mathcal{O} is 12 for photon absorption lengths of 0.9 μm . The KETEK SiPM yields the same number for absorption lengths of 0.4 μm . If the difference in absorption lengths is taken at face value, it follows that the avalanche region is located 0.5 μm deeper in the Hamamatsu SiPM than in the KETEK SiPM.

Two more observations are that a) in between absorption lengths 0.08 μm and 0.4 μm , \mathcal{O} changes little in the Hamamatsu SiPM, while it changes much more in the KETEK SiPM. And b) \mathcal{O} never reaches as high a value in the KETEK SiPM as in the Hamamatsu SiPM. We interpret both observations as evidence for a location of the avalanche region in the KETEK SiPM that is right below the surface and that already for 400 nm photons a significant fraction of photons absorb below the avalanche region. In the Hamamatsu SiPM, on the other hand, the volume in between the thin first anode implant and the avalanche region is depleted.

In that scenario it is expected that the spectral response peaks at lower wavelengths in the KETEK SiPM than in the Hamamatsu SiPM. That is indeed what we observe. Figure 2 shows the spectral response of the two devices. Below 400 nm, the higher PDE of the Hamamatsu SiPM can be explained with its thinner entrance window and, maybe, thinner first implant. The important aspect for our argument is that below 400 nm the PDE of both devices is offset by a roughly constant factor. The interpretation is that for each wavelength the same fraction of electrons and holes initiates a breakdown in both devices. Above 400 nm the picture changes. While the PDE continues to increase up to 450 nm for the Hamamatsu SiPM, it drops for the KETEK SiPM. That divergence is explained by a change from electron initiated breakdowns to hole initiated ones in the KETEK SiPM, which is due to an increasing fraction of photons that absorb below the avalanche region as the wavelength increases. In the Hamamatsu SiPM photons up to 450 nm still absorb mostly above the avalanche

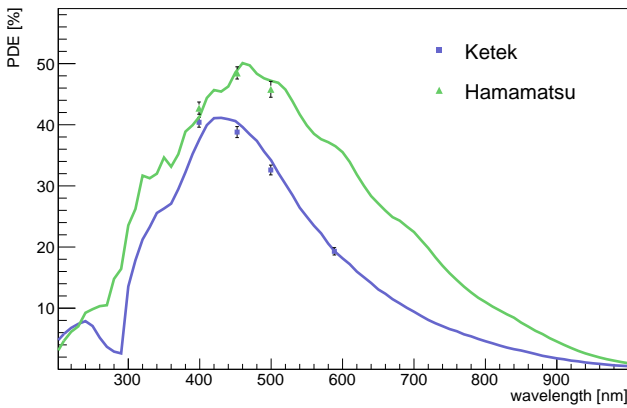


Figure 2: PDE vs. wavelengths of the two SiPMs from 200 nm to 1000 nm. For the measurement, the bias voltage for each devices is chosen such that the breakdown probability for 400 nm photons is 90%. The spectral response measurement is fit to the PDE measurements denoted by the data points.

region and, therefore, breakdowns remain mostly electron initiated.

4. Where Optical Crosstalk Photons enter a Cell

In this section we discuss how \mathcal{O} can be used to determine where optical crosstalk photons enter a cell. Optical crosstalk (OC) is caused by photons that are emitted in the breakdown of one cell and propagate into a neighboring cell where they initiate an additional breakdown. One distinguishes two types of OC (see e.g. [14]) In case the photon absorbs in the active (depleted) volume of a cell, the additional breakdown happens nearly simultaneous to the first breakdown, which is why that type of OC is called prompt or direct OC. If the photon is absorbed in a non-depleted region, e.g. in the bulk, the generated charges first have to diffuse into the depleted volume before they can initiate a breakdown . The diffusion time Δt can take several tens of nanoseconds depending on the distance d between the location of the photon absorption and the border to the active volume of the cell; $\Delta t \propto \sqrt{d}$. But it can also be just a fraction of a nanosecond if the photon absorbs close to the border.

How well the two types of OC can be separated depends on how well two subsequent pulses can be separated in the measurement. Any prompt OC measurement is thus always a combination of *true* prompt OC events and delayed OC events that have a time delay, which is below the capability of the measurement setup to resolve two overlapping pulses. Two pulses can be identified as such in our setup, if they are more than two nanoseconds apart.

Figure 3 shows the prompt OC of the two devices recorded at seven temperature between -75°C and 40°C . For the Hamamatsu device we discarded the measurement at 40°C because the contamination from pile-up of uncorrelated dark counts was too large and could not be reliably subtracted. For all other measurements the accidental

pile-up within a 2 ns time window could be subtracted by assuming that the time differences between dark counts are Poisson distributed. After the correction, all OC curves of one device fall on top of each other, as expected.

We now compare the OC of the two devices at the bias where the breakdown probability for 400 nm photons is 90%.³ The arrow in each panel marks the corresponding relative overvoltage. The KETEK device has a fairly high optical crosstalk of $\sim 20\%$, which is not surprising because it does not have trenches to prevent photons from propagating into neighboring cells. The prompt OC in the Hamamatsu device, on the other hand, is only 1.5%, which is an impressive improvement compared to past developments [10].

In [10] we showed that a valid model of the optical crosstalk vs. relative overvoltage is

$$OC(U_{\text{rel}}) = f \cdot C_{\text{eff}} \cdot U_{\text{rel}} \cdot U_{\text{BD}} \cdot \gamma \cdot \left[1 - e^{(-\mathcal{O} \cdot U_{\text{rel}})} \right] .(3)$$

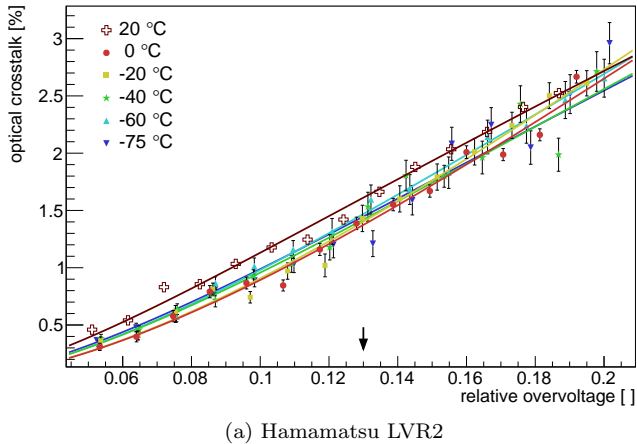
where we use $f = 3 \cdot 10^{-5}$ from [15] as the number of photons produced per charge carrier in the avalanche that can also cause OC. We note that other measurements of the photon intensity exist, e.g. [16, 17], but those also include spectral components, which are irrelevant for OC, either because the photon absorption lengths are too long (photons do not absorb in the device) or too short (photons absorb in the same cell they are emitted from). $C_{\text{eff}} \cdot U_{\text{rel}} \cdot U_{\text{BD}}$ is the gain of the SiPM, and γ is a figure of merit that quantifies what fraction of the photons produced in a breakdown make it into a neighboring cell. The term in square brackets is the breakdown probability already discussed in the previous section.

The OC data in Figure 3 are fit with that model. For the fit we fixed the cell capacitance C_{eff} at 84 fF and 154 fF and the breakdown voltage at 26.8 V and 37.5 V at 0°C , for the KETEK and Hamamatsu SiPM, respectively. The capacitance and breakdown voltages had been measured as described in [10]. The breakdown voltage is found to increase by about $0.1\%/\text{^{\circ}C}$ in both devices.

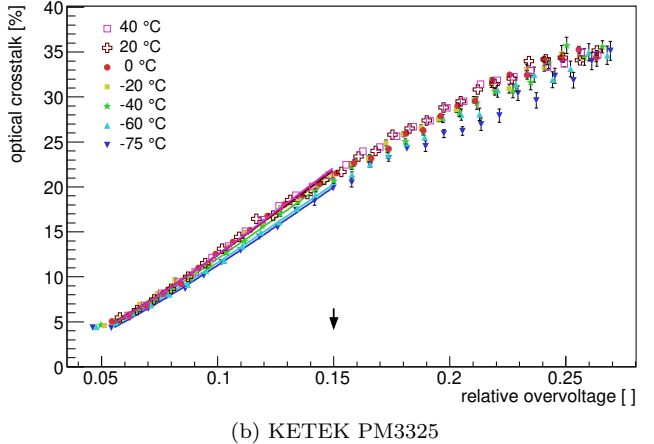
The Hamamatsu OC measurements can be fit over the entire measured range with an acceptable fit probability. For the KETEK device, we had to restrict the upper end of the fit range to a relative overvoltage of 0.15, i.e. OC of less than 20%, in order for the fit to yield an acceptable fit probability. It is evident from the KETEK data points, that the OC data turn over in what seems to be a saturating behaviour. An explanation for this behaviour is that for large OC of more than 20% and the cell size of the device, the probability of more than one OC photon absorbing in the same cell cannot be neglected anymore. That effect is not included in the fit model and would result in a flattening of the curve.

Table 2 lists the values for γ from the fits. The average values from our previously measured devices are also listed

³We do not imply that this operating point is optimal for an application but it allows for an unbiased comparison.



(a) Hamamatsu LVR2



(b) KETEK PM3325

Figure 3: Prompt optical crosstalk of the two tested SiPMs. The black arrow marks the relative overvoltage at which both devices yield a 90% breakdown probability for 400 nm photons.

Table 2: Best Fit Values for γ Obtained From Fitting the Prompt Optical Crosstalk Measurements Shown in Fig. 3. The Last Column Shows the Probability That a Photon Emitted in a Breakdown Makes it into a Neighboring Cell.

Device	Temp.	γ
Hamamatsu LVR2	-75°C	0.012±0.001
	-60°C	0.014±0.001
	-40°C	0.013±0.001
	-20°C	0.018±0.003
	0°C	0.017±0.001
	20°C	0.014±0.001
KETEK PM3325 WB	-75°C	0.347±0.009
	-60°C	0.355±0.008
	-40°C	0.378±0.009
	-20°C	0.384±0.007
	0°C	0.42±0.01
	20°C	0.415±0.008
	40°C	0.442±0.007
Hamamatsu LCT5		0.077±0.001
SensL J-Series		0.126±0.002
FBK NUV-HD		0.557±0.002

[10]. Comparing the numbers it is evident that the structure of the LVR2 device is 5.5 times better than the LCT5 device in preventing photons from crossing cells. The value for γ is 0.014, i.e. 1.4% of all photons make it into a neighboring cell where they can cause optical crosstalk. In the KETEK SiPM, between 35% and 44% of the photons cause optical crosstalk.

The second factor that determines the amount of OC is the product of breakdown voltage and cell capacitance, which is 2.25 pF·V for the KETEK and 5.78 pF·V for the Hamamatsu SiPM. It is a figure of merit that is proportional to the charge generated in an avalanche. This time it is the KETEK SiPM that outperforms the Hamamatsu device by a factor of 2.6 because of its smaller cell capacitance. However, the Hamamatsu SiPM has a two times smaller cell capacitance per cell area. We would thus expect that the product of cell capacitance and breakdown voltage for an LVR2 with 25 μm cells will be two times lower than for the KETEK device. This assumes that the cell capacitance scales linear with area, which is not necessarily the case as edge effects become important for small cell sizes.

The fit results also allow us to draw conclusions about where the crosstalk producing photons absorb relative to the avalanche region. For the previous generation of Hamamatsu SiPMs we could show that the majority of these photons absorb above the avalanche region [10]. That interpretation was confirmed by Hamamatsu, who found that these photons exit the silicon and reflect off the boundary between protective layer and ambient air back into a neighboring cell.

In the Hamamatsu SiPM studied here that contribution to prompt OC had been successfully suppressed by eliminating the protective epoxy layer. This is also what we find from the interpretation of \mathcal{O} . The best fit value for \mathcal{O} is about 10 ± 1 in all fits of the optical crosstalk. Comparing that value with the ones listed in Table 1 we conclude

that the breakdowns induced by optical crosstalk are hole initiated. This means that the photons absorb below the high-field region in a depth of $> 1 \mu\text{m}$ below the surface.

Three scenarios come to mind that can explain how optical crosstalk photons can absorb at such depths. The first scenario is that some photons manage to penetrate the trench between cells. That scenario is unlikely because photons would absorb uniformly across the cell, i.e. absorb above and below the avalanche region and, in consequence, result in values for \mathcal{O} larger than 10 because the occurring breakdowns are electron and hole initiated. The second scenario is that some photons with long absorption lengths still bounce off the air-SiPM interface and absorb deep inside the device, i.e. mostly below the avalanche structure.

The third, and our preferred, scenario is that photons cross into a neighboring cell below the trench. Either photons absorb in the bulk and the generated holes diffuse into the active volume within the 2 ns resolving time of our setup and are misidentified as prompt OC events. Or photons absorb in the active volume below the avalanche region and cause prompt OC.

The fit result for the KETEK SiPM yields an \mathcal{O} number of about 13 ± 0.7 . Comparing that value with the \mathcal{O} numbers in Table 1 lets us conclude that the majority of the photons absorb equally distributed across the avalanche region and thus produce an equal amount of electron and hole dominated breakdowns. That result is not surprising as the device does not have trenches in between cells, which would prevent photons to travel directly from the avalanche region where they are produced into a neighboring one.

5. Afterpulsing and Delayed Optical Crosstalk

If the prompt OC in the Hamamatsu device is indeed dominated by misidentified delayed OC, a reduction of the minority carrier lifetimes in the bulk or a better shielding of the active volume from carriers diffusing out of the bulk might be a viable way to reduce OC further, unless those measures are already implemented. We illustrate the potential room for improvement by discussing the delayed OC and afterpulsing characteristics of the two tested SiPMs.

Both quantities are extracted by recording time difference between SiPM pulses as explained in [10]. Afterpulsing events become dominant a few ten nanoseconds after a breakdown when the corresponding cell is recharged to 50% or more of its full capacity. Delayed OC signals dominate at shorter time differences. For the Hamamatsu LVR2 device the subjective division between the two contributions is made at 20 ns, and for the KETEK device at 10 ns. We note that our choice of separating the two contributions in the described way results in a contamination in each region with the opposite type of events, which, however, is acceptable for our purposes. Figure 4 shows

the afterpulsing and Figure 5 the delayed optical crosstalk probabilities of both devices.

The KETEK device has an afterpulsing probability of less than 1%, whereas the afterpulsing of the Hamamatsu device is two to three times larger, when compared at their respective bias, which yields a 90% breakdown probability for 400 nm photons (marked by the arrow in the figures). No significant temperature dependence is observed for both devices.

At the same overvoltages, the delayed OC changes from 0.01% at 40°C to 1% at -75°C for the KETEK SiPM. The temperature dependence is not that strong in the Hamamatsu SiPM, where the delayed OC is 3.5% at 20°C and increases by a factor of 1.3 to 4.5% at -75°C . We discard the delayed OC measurement at 40°C for the same reason we discarded the OC measurement at the same temperature.

Below relative overvoltages of 0.15, afterpulsing and delayed OC of the KETEK device are so low that the measurement is affected by systematic effects. Only at higher overvoltages is it possible to resolve the expected temperature dependence of the delayed optical crosstalk. The dependence is due to an increase of the carrier life times with decreasing temperatures.

The much lower delayed OC of the KETEK device makes us believe that the delayed OC in the Hamamatsu device can be reduced further and, if our interpretation of the origin of the prompt OC causing photons is correct, any such measure will simultaneously reduce the prompt OC. On the other hand it can be expected that future KETEK developments with trenches will be able to achieve a similar prompt OC performance as observed in the Hamamatsu SiPM.

6. Discussion

We parameterized the breakdown probability with a single quantity \mathcal{O} and used it to map the vertical structure of the avalanche region. We discussed how such a mapping can be used to learn about the origin of carriers relative to the avalanche structure.

The empirical mapping of the \mathcal{O} values obtained in PDE measurements to the photon absorption length allowed us to determine how far below the surface the avalanche region is located. However, because we have no access to the structure of the studied devices, we cannot verify the absolute accuracy of the mapping and the dependence of \mathcal{O} on the size of the avalanche region. To verify that assumption and for a more precise probing of the high-field structure, dedicated test structures are needed to calibrate the method. The main parameters to vary in these structures are the size of the region and its location below the surface. We hope that this paper inspires future work in that direction by groups that have access to appropriate structures.

The second application of \mathcal{O} we demonstrated is the identification of the origin of carriers relative to the loca-

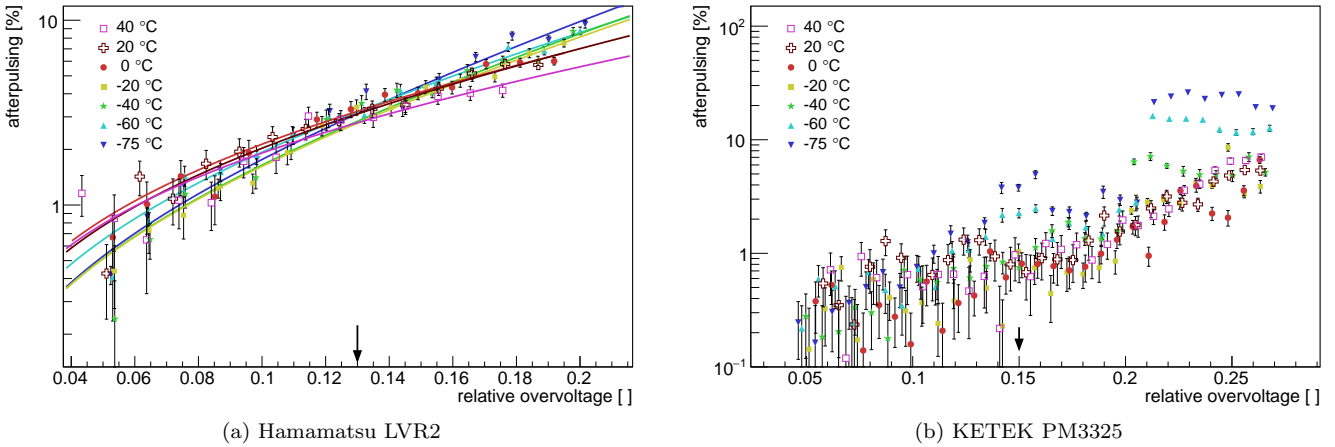


Figure 4: Afterpulsing probability of the two devices.

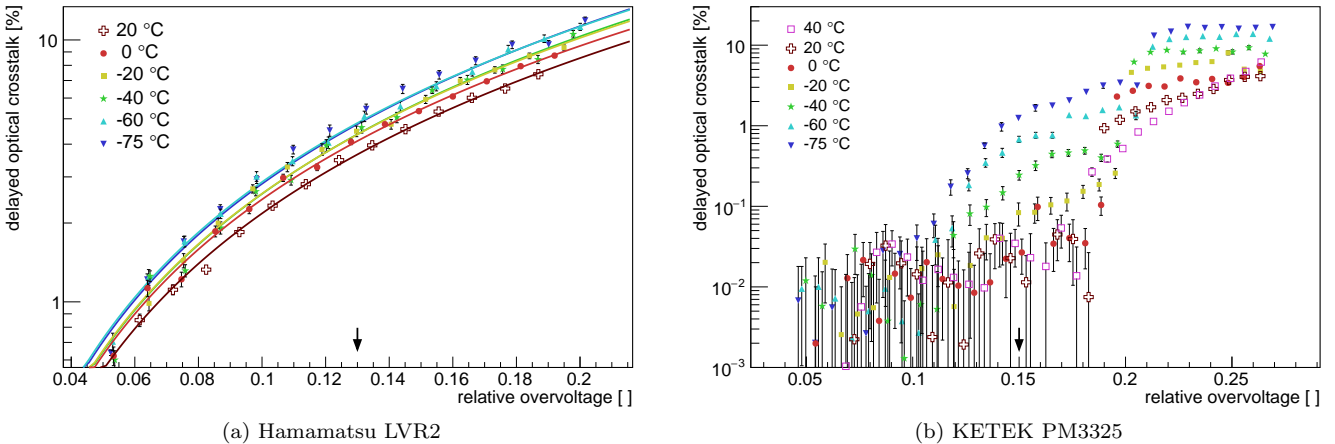


Figure 5: Delayed optical crosstalk of the two devices.

tion of the avalanche region. As an example we showed that the optical-crosstalk producing charge carriers enter the high-field region from below in the Hamamatsu LVR2 SiPM, whereas in the KETEK device, the optical-crosstalk photons *illuminate* the avalanche region of a neighboring cell from the side. This information will help to further improve the prompt OC performance in future devices. We are not aware of another experimental method that provides the same information.

\mathcal{O} can also be used to identify the spatial origin of charge carriers produced by delayed optical crosstalk, afterpulsing, and dark counts relative to the avalanche region. However, two requirements need to be fulfilled first. A valid model has to exist that properly describes the bias dependence of the characteristic of interest and includes the breakdown probability. And the measurement cannot be contaminated, like, for example, our delayed optical crosstalk measurement, which also includes some afterpulsing events. Unless, of course, the model takes these contaminations into account too.

In conclusion we have introduced a novel method to characterize SiPMs and other avalanche structures that operate in Geiger mode. The method helps to improve the performance of future SiPMs and it allows to gain unique insight into the functionality of SiPM.

Acknowledgment

We are grateful to Hamamatsu and KETEK, who have provided us with samples of their latest developments. This research was in part supported by the National Science Foundation under grant no. PHYS-1505228.

References

- [1] S. Ogawa, Liquid xenon calorimeter for MEG II experiment with VUV-sensitive MPPCs, Nuclear Instruments and Methods in Physics Research Section A: Accelerators, Spectrometers, Detectors and Associated Equipment 845 (2017) 528–532. doi:10.1016/J.NIMA.2016.06.085. URL <http://www.sciencedirect.com/science/article/pii/S0168900216306489>

- [2] F. Moreau, J. C. Vanel, O. Drapier, M. Gonin, A. Bonnemaison, A. Cauchois, Y. Geerebaert, S. Couturier-Le Quellec, Mass characterization of multi-pixel photon counters for the T2K 280 m near detector, Nuclear Instruments and Methods in Physics Research, Section A: Accelerators, Spectrometers, Detectors and Associated Equipment 613 (1) (2010) 46–53. doi:10.1016/j.nima.2009.11.042.
 URL <http://www.sciencedirect.com/science/article/pii/S0168900209022220>
- [3] E. J. Mannel, An SiPM based readout for the sPHENIX calorimeters, in: IEEE Nuclear Science Symposium Conference Record, IEEE, 2013, pp. 1–4. doi:10.1109/NSSMIC.2013.6829439.
 URL <http://ieeexplore.ieee.org/document/6829439/>
- [4] H. Anderhub, M. Backes, A. Biland, V. Boccone, I. Braun, T. Bretz, J. Bu??, F. Cadoux, V. Commichau, L. Djambazov, D. Dorner, S. Einecke, D. Eisenacher, A. Gendotti, O. Grimm, H. Von Gunten, C. Haller, D. Hildebrand, U. Horisberger, B. Huber, K. S. Kim, M. L. Knoetig, J. H. K??hne, T. Kr??henb??hl, B. Krumm, M. Lee, E. Lorenz, W. Lustermann, E. Lyard, K. Mannheim, M. Meharga, K. Meier, T. Montaruli, D. Neise, F. Nessi-Tedaldi, A. K. Overkemping, A. Paravac, F. Pauss, D. Renker, W. Rhode, M. Ribordy, U. R??ser, J. P. Stucki, J. Schneider, T. Steinbring, F. Temme, J. Thaele, S. Tobler, G. Viertel, P. Vogler, R. Walter, K. Warda, Q. Weitzel, M. Z??glein, Design and operation of FACT-the first G-APD Cherenkov telescope, Journal of Instrumentation 8 (6) (2013) P06008–P06008. doi:10.1088/1748-0221/8/06/P06008.
 URL <http://stacks.iop.org/1748-0221/8/i=06/a=P06008?key=crossref.215223ca70483ee275407a04fb44da8>
- [5] A. Otte, K. Meagher, T. Nguyen, M. Carroll, S. Hooper, K. Mckinney, S. Peet, Silicon photomultiplier integration in the camera of the mid-size Schwarzschild-Couder Cherenkov telescope for CTA, Nuclear Instruments and Methods in Physics Research, Section A: Accelerators, Spectrometers, Detectors and Associated Equipment 787 (2015) 85–88. doi:10.1016/j.nima.2014.11.026.
- [6] A. N. Otte, J. Barral, B. Dolgoshein, J. Hose, S. Klemin, E. Lorenz, R. Mirzoyan, E. Popova, M. Teshima, A test of silicon photomultipliers as readout for PET, Nuclear Instruments and Methods in Physics Research, Section A: Accelerators, Spectrometers, Detectors and Associated Equipment 545 (3) (2005) 705–715. doi:10.1016/j.nima.2005.02.014.
- [7] V. C. Spanoudaki, A. B. Mann, A. N. Otte, I. Konorov, I. Torres-Espallardo, S. Paul, S. I. Ziegler, Use of single photon counting detector arrays in combined PET/MR: Characterization of LYSO-SiPM detector modules and comparison with a LSO-APD detector, Journal of Instrumentation 2 (12) (2007) P12002–P12002. doi:10.1088/1748-0221/2/12/P12002.
 URL <http://stacks.iop.org/1748-0221/2/i=12/a=P12002?key=crossref.e10b977bd4b95190897aebb2163f748f>
- [8] M. Perenzoni, D. Perenzoni, D. Stoppa, A 64 ?? 64-Pixels Digital Silicon Photomultiplier Direct TOF Sensor With 100-MPhotons/s/pixel Background Rejection and Imaging/Altimeter Mode With 0.14% Precision Up To 6 km for Spacecraft Navigation and Landing, IEEE Journal of Solid-State Circuits 52 (1) (2017) 151–160. doi:10.1109/JSSC.2016.2623635.
 URL <http://ieeexplore.ieee.org/document/7756659/>
- [9] R. Agishev, A. Comer??n, J. Bach, A. Rodriguez, M. Sicard, J. Riu, S. Royo, Lidar with SiPM: Some capabilities and limitations in real environment, Optics and Laser Technology 49 (2013) 86–90. doi:10.1016/j.optlastec.2012.12.024.
- [10] A. N. Otte, D. Garcia, T. Nguyen, D. Purushotham, Characterization of Three High Efficiency and Blue Sensitive Silicon Photomultipliers, Nuclear Instruments and Methods in Physics Research Section A: Accelerators, Spectrometers, Detectors and Associated Equipment 14 (8) (2016) 1–21. arXiv:1606.05186, doi:<http://dx.doi.org/10.1016/j.nima.2016.09.053>.
 URL <http://arxiv.org/abs/1606.05186>
- [11] G. Zappal??, F. Acerbi, A. Ferri, A. Gola, G. Paternoster, V. Regazzoni, N. Zorzi, C. Piemonte, Study of the photo-detection efficiency of FBK High-Density silicon photomultipliers, Journal of Instrumentation 11 (11) (2016) P11010–P11010. doi:10.1088/1748-0221/11/11/P11010.
 URL <http://stacks.iop.org/1748-0221/11/i=11/a=P11010?key=crossref.b0de4efb86f2d245334693c679c4f821>
- [12] W. G. Oldham, R. R. Samuelson, P. Antognetti, Triggering Phenomena in Avalanche Diodes, IEEE Transactions on Electron Devices 19 (9) (1972) 1056–1060. doi:10.1109/T-ED.1972.17544.
 URL <http://ieeexplore.ieee.org/document/1477015/>
- [13] S. M. Sze, K. K. Ng, Physics of semiconductor devices, Wiley-Interscience, 2007.
- [14] P. Buzhan, B. Dolgoshein, A. Ilyin, V. Kaplin, S. Klemin, R. Mirzoyan, E. Popova, M. Teshima, The cross-talk problem in SiPMs and their use as light sensors for imaging atmospheric Cherenkov telescopes, Nuclear Instruments and Methods in Physics Research, Section A: Accelerators, Spectrometers, Detectors and Associated Equipment 610 (1) (2009) 131–134. doi:10.1016/j.nima.2009.05.150.
 URL <https://www.sciencedirect.com/science/article/pii/S0168900209010456>
- [15] A. Nepomuk Otte, On the efficiency of photon emission during electrical breakdown in silicon, Nuclear Instruments and Methods in Physics Research, Section A: Accelerators, Spectrometers, Detectors and Associated Equipment 610 (1) (2009) 105–109. doi:10.1016/j.nima.2009.05.085.
 URL <https://www.sciencedirect.com/science/article/pii/S0168900209010390>
- [16] A. Lacaita, M. Ghioni, F. Zappa, G. Ripamonti, S. Cova, Recent advances in the detection of optical photons with silicon photodiodes, Nuclear Inst. and Methods in Physics Research, A 326 (1-2) (1993) 290–294. doi:10.1016/0168-9002(93)90366-P.
 URL <http://linkinghub.elsevier.com/retrieve/pii/016890029390366P>
- [17] R. Mirzoyan, R. Kosyra, H. G. Moser, Light emission in Si avalanches, Nuclear Instruments and Methods in Physics Research, Section A: Accelerators, Spectrometers, Detectors and Associated Equipment 610 (1) (2009) 98–100. doi:10.1016/j.nima.2009.05.081.
 URL <https://www.sciencedirect.com/science/article/pii/S0168900209010377>